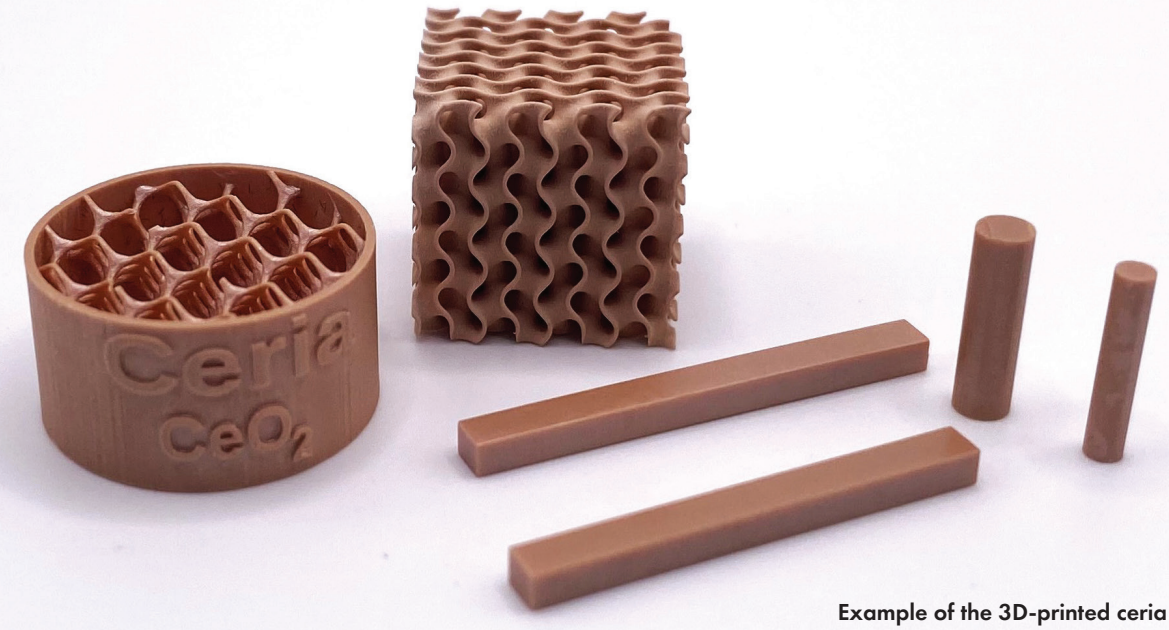

Example of the 3D-printed ceria ceramics investigated in this study.

Credit: Ryan Fordham

A study of lithography-based additive manufacturing of ceria ceramics

By Ryan Fordham, S. K. Sundaram, Shawn M. Allan, and Nicholas Voellm

Advances in additive manufacturing have led to a range of techniques to produce ceramics with complex geometries. This case study investigates the printability of ceria with a range of densities and microstructures using the Lithoz CeraFab 8500 system.

Cerium oxide, or ceria, is widely and historically known for its use as an abrasive, particularly to help polish specialized glasses,[1] such as telescope mirrors. But lately, this rare earth metal oxide has gained substantial attention in advanced technological applications as well, including photo- and electrocatalysis,[2,3] fuel cells,[4] and more recently, medicine.[5]

With respect to the medical industry, ceria has several properties of interest. It can absorb ionizing radiation,[6] making it a candidate for radiation shielding in medical imaging and radiation therapy. Ceria is also biocompatible and corrosion resistant,[7] so it can be used as a protective layer on implants, thus helping reduce the risk of inflammation, infection, and implant rejection. Additionally, the catalytic reactivity of ceria can be utilized in multiple medical processes, such as the degradation of pollutants for wastewater treatment or the detoxification of biological systems. Plus, if tailored for high surface area, ceria can adsorb or encapsulate drugs, thereby improving their stability, solubility, and bioavailability for controlled drug release applications.[8]

Various microstructural parameters and the thermal treatment of ceria have a large effect on its physical properties. However, achieving the desired geometry for ceria parts is difficult compared to metals and polymers. Where metals and polymers can be easily machined to achieve appropriate geometry, tolerance, and surface finish, the sensitivity of ceramics to flaws such as cracking, porosity, and crystalline defects makes machining these materials via traditional subtractive methods challenging.[9,10]

Recent advances in additive manufacturing (AM) have led to a range of techniques that can produce ceramics with complex geometries for niche applications. These processes include stereolithography, direct writing, robotic mate-

rial extrusion, and powder bed fusion.[11] Most AM systems for ceramics require a post-processing step to debind and densify the printed parts. The systems differ in how the printed parts are bound prior to densification.

Digital light projection (DLP) stereolithography is another AM technique that has long been used to additively manufacture ceramics. Compared to traditional stereolithography systems, which use a laser to trace a layer, DLP systems use a projected light source to cure an entire layer at once. Advancements in optics and image projection have allowed DLP systems to give very high lateral resolution while keeping processing times down compared to similarly powered stereolithography rastering laser systems.

The Lithoz CeraFab systems developed by ceramic additive manufacturer Lithoz GmbH (Vienna, Austria) is a subset of DLP stereolithography that has been patented for the proprietary Lithoz binder systems.[12] It employs a lithography-based ceramic manufacturing technique that utilizes a liquid-based, highly viscous photosensitive slurry to produce three-dimensional parts.[9]

The focus of this study was to investigate the printability of ceria with a range of densities and microstructures using the Lithoz CeraFab 8500 system. A parametric investigation was designed and implemented to determine the sensitivity of several processing parameters on the overall printability of ceria and the quality of the printed parts. The variables in the study were the ceramic powder particle size, solid loading of the printable slurry, and sintering temperature. Each parameter was varied at three levels spanning the expected workable range for that variable.

Materials and processing setup

Advanced Abrasives Corporation (Pennsauken, N.J.) supplied ceria powders with advertised purity of 99.95% and advertised particle sizes of 0.5 µm, 1 µm, and 2 µm. The powder was characterized using density measurements, particle size analysis, X-ray diffraction, and scanning electron microscopy to confirm phase, purity, and particle geometry. While the advertised and measured particle sizes for the 0.5 µm and 2 µm powders were fairly close, the 1 µm advertised powder measured an average particle size of 2.00 µm (Table 1).

Table 1. Powder particle size measurements of 0.5, 1, and 2 µm advertised ceria powders.

Advertised particle size (µm)	Measured average particle size (µm)	Standard deviation (µm)
0.5	0.547	0.547
1.0	2.003	0.960
2.0	1.926	0.879

Credit: Ryan Fordham

Slurry development was completed at Lithoz America LLC (Troy, N.Y.). The liquid-based slurry comprised a suspension of ceria powder in a photosensitive resin. The resin was a mixture of photoinitiators, low molecular weight monomers, and dispersants. A combination of a light-emitting diode array and a digital micromirror device was used to selectively polymerize the resin. The printing light intensity was reduced to 300 mJ/cm^2 to avoid overpolymerization.

Grindometer measurements were carried out for each slurry formulation to identify large particles and agglomerates in the slurry. Each particle size batch was then mixed with a proprietary binder system, and the rheology was tracked as the solid loading was increased. Once the slurry reached a loading that caused significant shear thickening, the slurry was deemed unusable. The maximum loading, prior to shear thickening behavior, was used as the medium value for the study. An increase of 2 vol.% and a decrease of 2 vol.% were used for the high and low study values, respectively. Based on the rheology of the slurries for the 0.5, 1, and 2 µm powders, maximum workable solid loadings were 39, 39, and 41.5 vol.%, respectively. It was recommended that the slurry be kept in cold storage to avoid self-polymerization.

Ideal sintering temperature was determined by sintering five cold pressed ceria pellets at increasing temperatures between 1,400°C and 1,600°C. The optimal sintering temperature was found to be 1,450°C. After this determination, a print schedule was prepared to organize the print runs and optimize for printing time. Each print consisted of six cylinders, each 0.5 cm in diameter and 0.25 cm tall. Following 3D printing, the six parts were separated into three pairs and each pair was preconditioned, debinded, and sintered together. The prints were completed at a raised ambient temperature of 29.5°C.

After processing, all ceria samples underwent bulk and surface characterization. Density was measured using the Archimedes immersion method, following the American Standards and Testing Methods standard C20-00. Scanning electron microscopy micrographs were used to analyze the microstructures of the printed samples. Charging occurred on the surface of the lower density samples, and therefore images were not taken at high magnifications for those samples. Grain boundaries were clearly visible and used for grain size measurements.

Variations in sintering schedules, as well as the addition of dopants, such as gadolinium, have been known to affect the reduction of ceria.[13–17] So, X-ray photoelectron spectroscopy was used to measure the fractional oxidation states of cerium in the printed samples sintered at a single selected sintering temperature. From the measured data, no significant variation in cerium oxidation was found between the samples. The small amount of Ce(III) that was found (~5.5%) could be attributed to charging of the samples from the X-ray source or the ultrahigh-vacuum environment during the measurement.

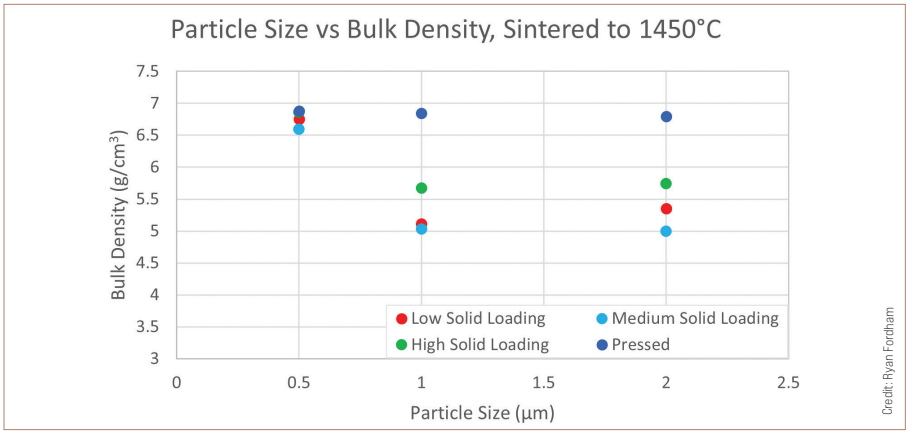

Figure 1. Effect of particle size on the bulk density of ceria sintered at 1,450°C.

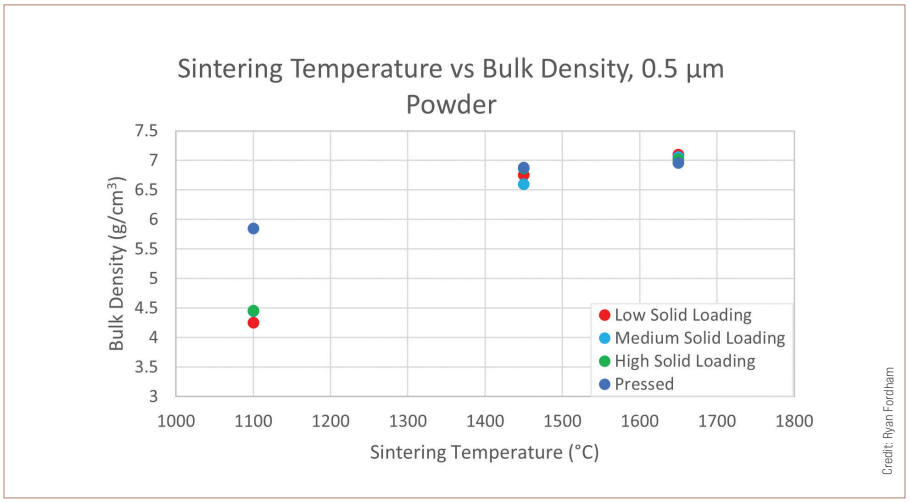

Figure 2. Effect of sintering temperature on bulk density of ceria 0.5 µm particle size.

Results and discussion

Parametric effects on bulk density

Figure 1 shows the effect of powder particle size on the bulk density of printed parts. The bulk density for the pressed pellets was constant between each particle size; however, it increased from about 5.8 g/cm^3 for parts sintered at 1,450°C to about 7.0 g/cm^3 for parts sintered at 1,650°C. In every instance for the printed samples, the 0.5 µm particle size samples sintered to a higher density than the comparable 1 µm and 2 µm samples, and the pressed samples were also significantly higher density than the printed samples when sintered at the low sintering temperature of 1,100°C.

The difference in density between the pressed and printed samples is due to the difference in packing density of the powder prior to sintering. The minimal difference between the density of the 1 µm and 2 µm powder samples also suggests the particle size measurements were accurate, and the 1 µm advertised powder has an actual particle size of about 2 µm.

As expected, the bulk density of each sample increased with sintering temperature (Figure 2). The 0.5 µm powder reached the highest bulk density at about 7.1 g/cm^3, and the 1 µm and 2 µm powders were slightly less dense at a maximum of about 6.7 g/cm^3. The 0.5 µm powder also showed a consistent density between each solid loading, including the pressed samples, when sintered at the medium and high temperatures. The 1 µm and 2 µm printed samples were all found to be less dense than the pressed samples, even at the highest sintering temperature of 1,650°C.

The narrow range of solid loadings chosen for this study had no significant effect on the final parts' bulk density.

Parametric effects on microstructure

No significant changes in microstructure were found with the narrow range of solid loading that was investigated. However, particle size and sintering temperature showed a wide range of porosity and grain size.

Figure 3 shows the effect of particle size and sintering temperature on the microstructure. As expected, the samples sintered at 1,100°C have open pores running through the sample. Small grains are visible, with some coalescing of the particles evident at this low sintering temperature. The samples sintered at 1,450°C show higher density material with visible grain boundaries. Open pores can still be seen throughout the samples printed with 1 µm and 2 µm powders. The samples sintered at 1,650°C show a reduction in porosity and pore size and exaggerated grain growth.

Intragranular porosity was also seen on the surface of the printed parts. This porosity is caused by larger starting grains in the 1 µm and 2 µm powders. As the sintering temperature is increased, the intergranular pores are trapped during the accelerated grain growth and thus becoming intragranular. This porosity is only seen in the 1 µm and 2 µm powder samples sintered at the highest temperature of 1,650°C.

Parametric effects on grain size

Average grain size of the printed samples was strongly dependent on the particle size of the ceria powder used in the slurry as well as the sintering temperature. Because of the higher surface area and therefore higher surface energy of the 0.5 µm powder, these samples consistently had larger grain sizes than the comparable 1 µm and 2 µm powder samples. Solid loading showed an effect on the 0.5 µm powders but there was no significant change in the 1 µm and 2 µm powder samples. As expected, sintering temperature showed a strong positive correlation with average grain size.

Summary and conclusions

In this study, we established the processing parameters for ceria ceramics produced via lithography-based 3D printing. The powder characterization in addi-

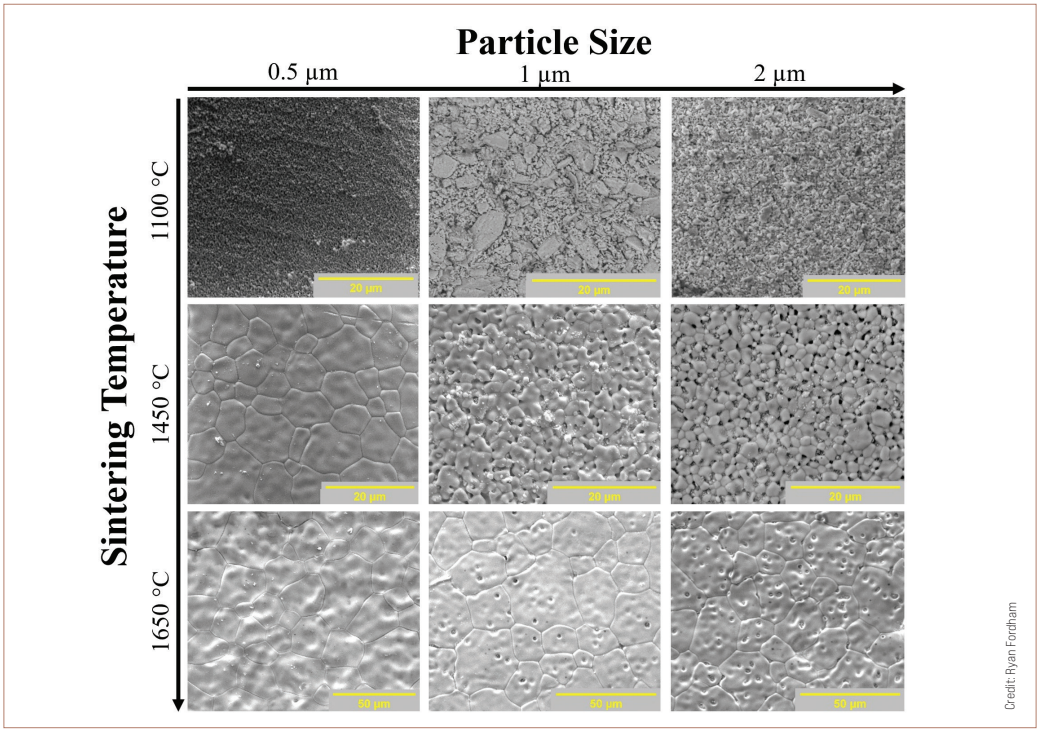

Figure 3. Effect of particle size and sintering temperature on the microstructure of 3D-printed ceria.

tion to the observations made through the sintering study of the pressed pellets were consistent with other conventionally manufactured ceria. Based on the density and microstructure, usable values for particle size, sintering temperature, and solid loading were found for additive manufacturing of ceria.

Powder particle size and sintering temperature were found to have a prominent effect on the bulk density and microstructure of the printed samples. Ultimately, based on the particle sizes investigated in this study, 0.5 µm particle size ceria powder with a slurry solid loading of 41.5 vol.% and sintering temperature of about 1,450°C is recommended for production of high-density ceria ceramics with complex structures and geometries. Further investigations of sintering temperature and time may lead to reduced grain growth while producing a high-density solid. But in any case, these results help enable the advancement of AM of ceria and ceria-containing materials.

About the authors

Ryan Fordham, Shawn M. Allan, and Nicholas Voellm are materials engineer, vice president, and materials technician, respectively, at Lithoz America (Troy, N.Y.). S. K. Sundaram is an Inamori Professor of materials science and engineering at Alfred University in New York. Contact Fordham at rfordham@lithoz-america.com.

References

[1]Z. Zhang et al., "Surface modification of ceria nanoparticles and their chemical mechanical polishing behavior on glass substrate," *Appl. Surf. Sci.* 2010, **256**(12), 3856–3861.

[2]M. Stojmenović et al., "Electrical characterization of multidoped ceria ceramics," *Ceram. Int.* 2013, **39**(2), 1249–1255.

[3]R. J. Gorte, H. Kim, and J. M. Vohs, "Novel SOFC anodes for the direct electrochemical oxidation of hydrocarbon," *J. Power Sources* 2002, **106**(1–2), 10–15.

[4]A. J. Jacobson, "Materials for solid oxide fuel cells," *Chem. Mater.* 2010, **22**(3), 660–674.

[5]F. Pagliari et al., "Cerium oxide nanoparticles protect cardiac progenitor cells from oxidative stress," *ACS Nano* 2012, **6**(5), 3767–3775.

[6]S. Yalcin et al., "Radiation shielding properties of cerium oxide and erbium oxide doped obsidian glass," *Radiat. Phys. Chem.* 2019, **160**: 83–88.

[7]Y. Xiong et al., "Characterization and electrochemical corrosion behavior of biological ceramic coatings on magnesium alloy by micro-arc oxidation," *Journal of Biobased Materials and Bioenergy* 2014, **8**(2): 158–164.

[8]S. Das et al., "Cerium oxide nanoparticles: Applications and prospects in nanomedicine," *Nanomedicine* 2013, **8**(9): 1483–508.

[9]M. Schwentenwein, P. Schneider, and J. Homa, "Lithography-based ceramic manufacturing: a novel technique for additive manufacturing of high-performance ceramics," *Adv. Sci. Technol.* 2014, 60–64.

[10]Z. C. Eckel et al., "Additive manufacturing of polymer-derived ceramics," *Science* 2016, **351**(6268), 58–62.

[11]D. L. Bourell and C. E. R., "Photonics applied: 3D laser printing: Selecting and using materials for additive manufacturing processes," *Laser Focus World* 2016. https://bit.ly/3N7GYG3

[12]H. Johannes et al., "Method for the layered construction of a shaped body," U.S. Patent 10967564B2, March 2016.

[13]C. Nicollet et al., "Gadolinium doped ceria interlayers for solid oxide fuel cells cathodes: Enhanced reactivity with sintering aids (Li, Cu, Zn), and improved densification by infiltration," *J. Power Sources* 2017, **372**: 157–165.

[14]C. M. Sims et al., "Approaches for the quantitative analysis of oxidation state in cerium oxide nanomaterials," *Nanotechnology* 2018, **30**(8), 085703.

[15]S. M. Ali et al., "Effect of sintering temperature on surface morphology and electrical properties of samarium-doped ceria carbonate for solid oxide fuel cells," *Ceram. Int.* 2015, **41**(1), 1323–1332.

[16]S. Kazlauskas et al., "Effect of sintering temperature on electrical properties of gadolinium-doped ceria ceramics," *J. Mater. Sci.* 2015, **50**(8), 3246–3251.

[17]F. Zhang et al., "Cerium oxidation state in ceria nanoparticles studied with X-ray photoelectron spectroscopy and absorption near edge spectroscopy," *Surf. Sci.* 2004, **563**(1–3), 74–82.